International Journal of Nanomedicine

Dovepress
open access to scientific and medical research

Open Access Full Text Article

ORIGINAL RESEARCH

Combination of Chlorambucil and Mercaptopurine Show Effective Anti-Cancer Effects in Mice Model

Weibing Xu[1], Yuxin Di[1], Shengjing Chu[1], Zixuan Wang[1], Haitao Long[1], Lumei Pu[1], Runtian Ma[1], Yanwei Wang[2]

[1]College of Science, Gansu Agricultural University, Lanzhou, 730000, People's Republic of China; [2]Department of Chemical and Materials Engineering, School of Engineering and Digital Sciences, Nazarbayev University, Astana, 010000, Kazakhstan

Correspondence: Weibing Xu, College of Science, Gansu Agricultural University, No. 1 Yingmen Village, Anning District, Lanzhou, 730000, People's Republic of China, Tel/Fax +86 931 7631212, Email xuwb@gsau.edu.cn

Background: Combination therapy employing multiple drugs has been shown to enhance the efficacy of cancer treatment. Chlorambucil (Chl) and 6-mercaptopurine (6MP) are the first-line medicines for chronic lymphocytic leukemia and ovarian cancer. However, both were limited by their short half-life of disintegration, unsatisfactory water solubility, and adverse reactions.

Methods: In this work, the drug Chl and 6MP were introduced into the polymerized N-(2-hydroxypropyl) methacrylamide (polyHPMA) by pH and glutathione responsive linker to construct the polymer nanodrug delivery system for effective co-delivery.

Results: The drug load capacities, release, morphology, and cytotoxicity of the pro-drug were systematic. The two drugs showed satisfactory synergism with a combination index of 0.81, and a better ability to induce apoptosis. In and ex vivo fluorescence imaging showed a rapid systemic distribution of the conjugate within mice, majorly metabolized by liver and kidneys and eliminated after 24 hr. No significant pathological damage was observed in the major organs. This polymeric prodrug system holds promise for improved therapeutic efficiency and reduced side effects through the synergistic delivery of various chemotherapeutics.

Conclusion: The introduction of HPMA as a carrier not only enhanced the solubility and biocompatibilities of Chl and 6 MP but also improved their drug effect. This strategy might be a promising alternative for constructing multi-drug-release system.

Keywords: polymer prodrug, co-delivery, chlorambucil, mercaptopurine, fluorescence images, cancer treatment

Introduction

Multi-drug combination therapy, which outperforms single-agent therapies, has become a pivotal strategy in treating a variety of cancers.[1,2] This therapeutic approach offers increased efficacy, allows for dosage reduction while maintaining equal or superior efficacy, and mitigates drug resistance.[3–5] The strategy of combining structurally different drugs through physical encapsulation, covalent conjugation, and/or self-assembly has been extensively studied. A plethora of carrier materials, including liposomes, polymers, silicon nanoparticles, and dendrimers, are employed in multi-drug co-delivery systems. Liao et al prepared doxorubicin (DOX)- and camptothecin (CPT)-conjugated macromolecular monomers and a platinum (Pt)-conjugated crosslinker.[6] They then developed nanoscale bio-star polymers containing three drugs (cisplatin, DOX, and CPT) via ring-opening metathesis polymerization, using optimal ratios of drug-macromolecular monomers (MMs), crosslinkers, and catalysts. This enabled the unmodified drugs to be released from the nanoparticles through three different triggers: hydrolysis, UV exposure, and redox reactions.[6] The polymerization method was also utilized to produce "bottlebrush prodrugs" that included a tri-drug combination comprising bortezomib, pomalidomide, and dexamethasone, which act as proteasome inhibitors, immunomodulators, and corticosteroids, respectively.[7]

Chlorambucil (Chl) is the main chemotherapy drug for chronic lymphocytic leukemia and ovarian cancer.[8,9] Its mechanism of action involves the formation of covalent bonds with DNA bases, leading to the disruption of DNA replication and consequently impeding the growth of cancer cells.[10,11] Moreover, for many years, 6MP has been the

Received: 2 October 2023
Accepted: 16 December 2023
Published: 29 December 2023

Graphical Abstract

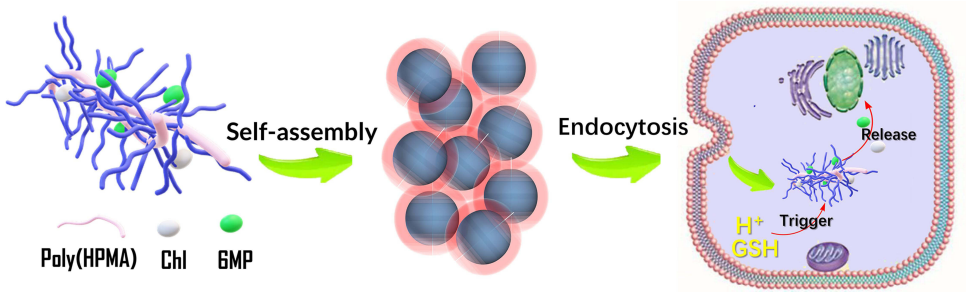

preferred medication for treating acute lymphoblastic leukemia.[12,13] It is believed that its biological activity is mediated through various modulations of cellular metabolism. The binding of 6MP metabolites to nucleic acids is the main pathway for its activity.[14,15] However, the nude drugs of Chl and 6MP are faced with the difficult situation of a short half-life for disintegration, limited water solubility, and significant adverse effects.[16–19] A meticulous literature review reveals that both of the aforementioned pharmaceuticals exert their inhibitory effects on cancer cell proliferation by disrupting the replication of the genetic material within cancer cells. In other words, these two drugs share a common mechanism of action. Additionally, they encounter analogous challenges, such as low drug utilization efficiency. Despite the successful development of numerous targeted delivery systems for Chlorambucil (Chl) or 6-Mercaptopurine (6MP), which have significantly enhanced their bioavailability while reducing side effects, there is currently a lack of reported research on the co-encapsulation of these two drugs, which share essentially identical binding sites, within the same delivery system. Such an approach has the potential to overcome their common challenges and, in a synergistic co-delivery manner, enhance the efficacy of these drugs.

Among the many polymer carriers, the homopolymer obtained by polymerizing N-(2-Hydroxypropyl) methacrylamide monomer, known as polyHPMA, exhibits favorable characteristics such as water solubility, non-immunogenicity, non-toxicity, and biocompatibility. More importantly, polyHPMA showed excellent anti-protein contamination properties compared to other drug carriers (eg poly(carboxybetaine acrylamide) and PEG) when it was exposed to human fluids (cerebrospinal fluid, saliva, and urine) and animal fluids (chicken egg and whole cow milk).[20] The hydroxyl group attached to the polymer can be designed to link a variety of different drugs or target ligands to create delivery systems that perform different functions.[21,22] However, multi-drug combined delivery systems based on polyHPMA are rarely reported.

Building on the solid foundation of our previous research about polyHPMA base drug delivery research for a long time, a co-delivery system incorporating Chl and 6MP with polyHPMA as the carrier was successfully prepared. After rigorous and systematic characterizations, the prepared co-delivery system is found to have a satisfactory synergism with a combination index of 0.81, and with a better ability to induce apoptosis. Comparing with the single-drug delivery systems, co-delivery systems enhanced their effectiveness in promoting tumor cell apoptosis, suggesting their potential for improved therapeutic outcomes. Furthermore, the co-delivery system is demonstrated with rapid distribution in vivo, fast metabolic rate, and satisfactory security. This work not only proves the superiority of combined drug delivery but also provides a feasible template for the co-delivery of various chemotherapeutics.

Materials and Methods

N-(2-hydroxypropyl)methacrylamide (HPMA), triethylborane (1.0 M solution in tetrahydrofuran), chlorambucil, mercaptopurine, dithiothreitol (DTT), dicyclohexylcarbodiimide (DCC), 4-dimethylamino-pyridine (DMAP), and propiolic acid were obtained from Macklin Bio-Chem Technology Co., Ltd. Formaldehyde solution (37 wt%) was bought from Yan tai Shuang Shuang Chemical Co., Ltd. Ammonia solution (25 wt%) was purchased from Tianjin Baishi Chemical Co., Ltd. 3-(4,5-Dimethylthiazol-2-yl)-2,5-diphenyltetrazolium bromide (MTT), RPMI1640 medium, fetal bovine serum

(FBS), and dimethyl sulfoxide (DMSO) were procured from Beijing Solarbio Science & Technology Co., Ltd. The above materials can be used without further treatment.

HepG2 cells, adult rabbits weighing about 2 kg and healthy male Kunming mice (20 ± 2 g) came from College of Veterinary Medicine, Gansu Agricultural University. The cells were authenticated by STR profile. The cell and animal experimental procedures are in accordance with the provisions of the "Experimental Animal Care and Use Guide" and have been reviewed and approved by the Animal Ethics Committee of Gansu Agricultural University.

The cis-3- (9H-purin-6-ylthio) acrylic acid (PTA) was a 6MP prodrug, which undergoes an addition-elimination reaction with glutathione (GSH) to yield 6MP in the tumor cell.[23] Although the conjugate was constructed by the reaction of PTA and polyHPMA in this experiment, the conjugate released 6MP under the stimulation of GSH.

The poly(HPMA)-Chl-PTA was fabricated as following: 200 mg of poly(HPMA), 40 mg of Chl, and 30 mg of carboxylated derivative 6MP (PTA) were completely dissolved in 2.0 mL of DMSO. Then, the solution was cooled to 0°C under a cold trap. Forty-five milligrams of DCC and 10 mg of DMAP were added to the above solution, and kept stirring for 48 hr under nitrogen protection at room temperature. By adding acetone and ether, the precipitate was filtered from the solution and then dissolved in methanol. The solution was subjected to dialysis for 48 hr, resulting in the formation of poly(HPMA)-Chl-PTA. Poly(HPMA)-Chl and poly(HPMA)-PTA were prepared with a similar method, and the PTA and Chl were removed in the process.

The annexin V-FITC apoptosis assay kit was employed to quantitatively detect apoptotic and necrotic cells to evaluate the cell death mechanism. The cell culture procedure parallels that of the MTT assay. Cells were collected into centrifuge tubes, after which 300 μL of binding solution was introduced to each tube. Then, 5 μL of Annexin-V was added to each tube. After shielding from light for 15 min, 10 μL of PI was added, and the tubes were shielded from light again for 5 min. For the cycle assay, after the cells were incubated with the conjugates for 24 hr, the medium was collected into centrifuge tubes, and the cells underwent digestion with trypsin in each well. Following centrifugation at 1500 r for 5 min, the supernatant was discarded. Thereafter, EDTA-Na_2 and RNAase were added, and the mixture was left for 5 min at room temperature. Subsequently, Triton X-100 and PI solution were added, and the samples were shielded from light for 10 min and were then examined microscopically on a flow cytometer.

In and ex vivo fluorescence imaging of the nanoparticles was performed in mice and their major organs. The Cy5.5 labeled conjugate was dispersed in PBS with the aid of ultrasound to form a solution with a concentration of 10 mg/mL. Healthy male Kunming mice were randomly divided into two groups (n = 3). One group received the conjugate via a tail vein injection (20 μL injection volume, at a dose of 20 g/kg). The control group was administered PBS. The imaging was collected at specific time points: at pre-injection, 6.0 and 24.0 hr post-injection.

Results and Discussion

The preparation process is shown in Figure 1a. Poly(HPMA) was prepared using a convenient RAFT polymerization process in an air atmosphere.[24] Subsequently, 6MP was modified by carboxylation to obtain its prodrug, PTA. Chl and PTA were directly anchored to the hydroxyl group of poly(HPMA) via esterification and catalyzed by DCC. For comparative purposes, poly(HPMA)-Chl and poly(HPMA)-PTA were also fabricated using similar methods.

The chemical structures of both free drugs and three conjugates were characterized by 1H NMR (Figures S1 and S2). The chemical shifts of each hydrogen atom are labeled.[25,26] The characteristic signals of Chl, PTA, and HPMA units can be found in the Poly(HPMA)-Chl-PTA conjugate, indicating that both drugs are bonded to the poly(HPMA) carries successfully. A semi-quantitative estimation of 6MP and Chl loading in the poly(HPMA)-Chl-PTA conjugate is achieved by determining the ratio of integrated areas corresponding to specific protons. This includes the -S-CH=CH- proton in PTA units (at 6.43 ppm), the benzene proton in Chl units (at 6.66 ppm), and the CH_3-C*H*(OH)- proton (at 3.68 ppm) in the poly(HPMA) backbone. It was found that the poly(HPMA)-Chl-PTA conjugate contained 14.5% and 11.2% of 6MP and Chl on average, respectively. The characteristic UV absorption peaks of the Chl and PTA groups at maximum wavelengths of 263 and 322 nm are simultaneously visible in poly(HPMA)-Chl-PTA conjugate (Figure S3). The absorbance curves of the solutions containing the three conjugates were analyzed against a calibration curve to quantify the content of 6MP and Chl groups. The content of 6MP was about 10.3% and 11.2% in poly(HPMA)-PTA and poly(HPMA)-Chl-PTA conjugates, respectively. The content of Chl was about 10.8% and 10.5% in poly(HPMA)-Chl

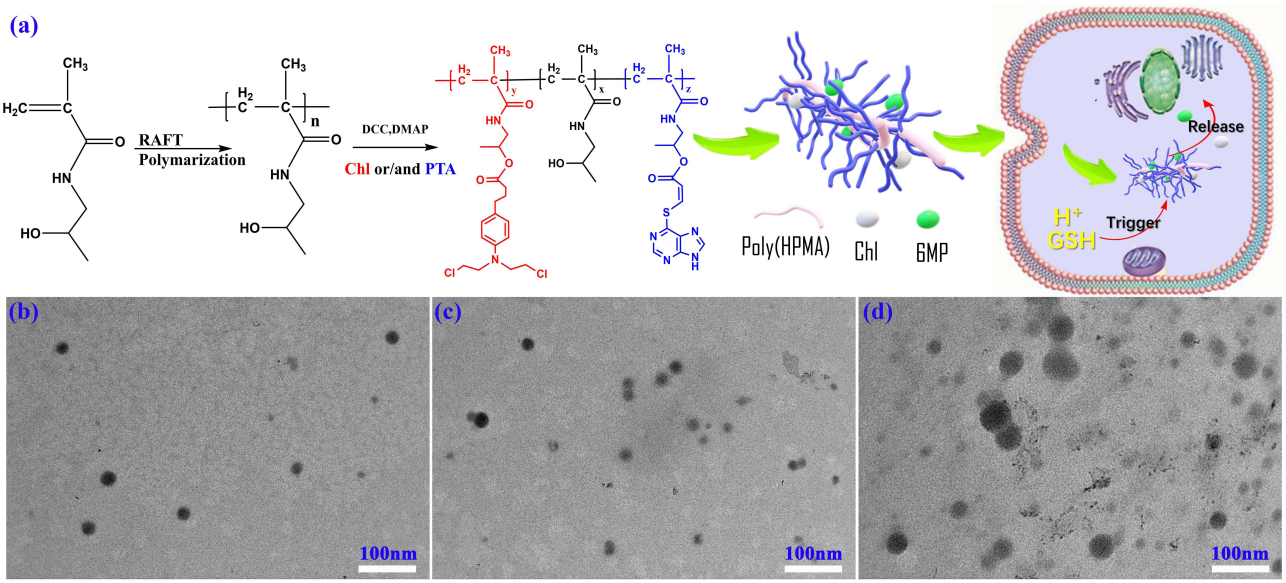

Figure 1 (**a**) Synthetic routes of the Poly(HPMA)-Chl-PTA conjugates; TEM images showing the morphology of the nanoparticles of (**b–d**) of poly(HPMA)-Chl, poly (HPMA)-PTA and poly (HPMA)-Chl-PTA conjugates.

and poly(HPMA)-Chl-PTA conjugates, respectively. FTIR analysis was applied to characterize the chemical constitution of the conjugates, and the results are shown in Figure S4a, and the detailed discussion was listed in the supporting information. The characteristic peaks of both Chl and PTA are clearly shown in the spectra of Poly(HPMA)-Chl (red line) and Poly(HPMA)-PTA (black line), respectively.[27,28] Furthermore, the characteristic peaks of Chl and PTA could be found simultaneously in the spectra of Poly(HPMA)-Chl-PTA. In addition, TGA and DTG have also demonstrated the successful preparation of the compound conjugates (Figure S4b and c).[29,30] The size of Poly(HPMA)-PTA and poly (HPMA)-Chl was found to be 95.68 nm and 80.2 nm on the first day (Figure S4d), respectively. The values decreased to 89.34 nm and 78.56 nm on the fifth day. The size of poly(HPMA)-PTA-Chl was 195.78 nm on the first day. The increase in the size of poly(HPMA)-PTA-Chl may be attributed to the increased content of hydrophobic components in the conjugate. Over the course of five consecutive days, the surface charge of all three conjugates changed by less than 2%, indicating good solution dispersibility and stability (Figure S4e). MALDI-TOF analyses of the poly(HPMA)-Chl-PTA conjugate showed a single series of molecular weights.[31] The central peak for the conjugate is at 9379 amu. This suggests that the number-averaged molecular weights of the conjugate are ~10,000 kD (Figure S4f).

The microstructure of the three conjugates was observed by transmission electron microscopy (Figure 1b–d). It can be clearly observed that all three conjugates are spherical in shape. This is due to the fact that the three conjugates are amphiphilic and can easily self-assemble into nanostructures in aqueous solutions. The self-assembly is driven by the hydrophobic interactions and π-π stacking interactions and the abundant presence of aromatic rings in the conjugates. The diameter of the particles formed by poly(HPMA)-PTA and poly(HPMA)-Chl ranged from ~50 to 70 nm, while that of poly(HPMA)-Chl-PTA ranged from ~100 to 120 nm. The diameter measured by TEM is significantly smaller than that measured by the particle size analyzer, which is due to the fact that TEM measured the dry state of the sample.

The release of the three conjugate solutions was examined using the UV–Vis method under pH = 5 and DTT solution. The results are shown in Figure 2. Since Chl is directly linked to poly(HPMA) via ester bonds, the release of the poly(HPMA)-Chl conjugate is tested under pH = 5 and 7.4 in PBS solution without DTT. The cumulative release of Chl at pH = 5 and 7.4 was 60.2% and 7.5% after 25 hr (Figure 2a), respectively. The pH of the conjugate solution was adjusted to 1 with concentrated hydrochloric acid after 25 hr; it was then left for 30 min, subsequently dialyzed into water for 3 days, and finally freeze-dried for UV testing (Figure 2b). It can be seen that the characteristic UV absorption of the Chl group is completely absent from the treated residue. This indicates that Chl units linked to the conjugate by ester bonds can indeed be released under acidic conditions. This result was also confirmed by TEM images of the residue

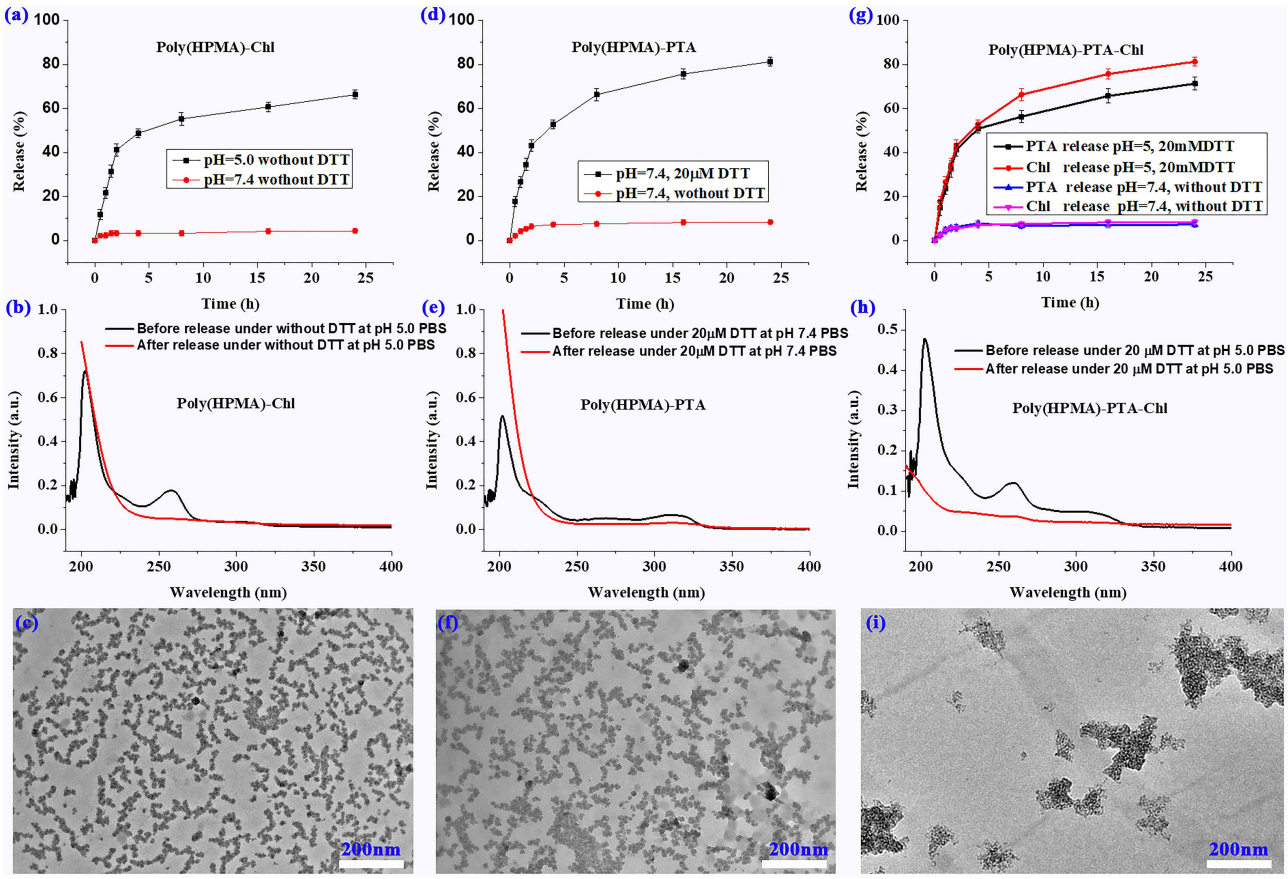

Figure 2 Release behaves under various condition (**a, d** and **g**), the UV absorption curves before and after release (**b, e** and **h**), and TEM images of the residue after release (**c, f** and **i**) of poly (HPMA)-Chl, poly (HPMA)-PTA and poly (HPMA)-Chl-PTA conjugates.

(Figure 2c). TEM images of the post-release residue show a smaller petal-packed structure, having lost the pre-release spherical structure completely. This is due to the release of hydrophobic drug groups, resulting in the destruction of the amphiphilic structure of the conjugate, thus losing the driving force of self-assembly. The 6MP was covalently linked to poly(HPMA) via a glutathione-responsible carbonyl vinyl sulfide bond. The release of the poly(HPMA)-PTA conjugate was tested both with and without DTT in PBS solution at pH = 7.4. The cumulative release of 6MP at 0 and 20 μM DTT was 81.2% and 9.5% after 25 hr (Figure 2d), respectively. The concentration of DTT was adjusted to 1.0 mmol and was maintained for 30 min after 25 hr of continuous detection; then the solution of the conjugate was freeze-dried after 3 days of water dialysis. The UV curves of Poly(HPMA)-PTA before release and the residue after release are shown in Figure 2e. It can be seen that the characteristic absorption band at 322 nm of 6MP in the residue after release has completely disappeared. The morphology of the residue after release is similar to that of poly(HPMA)-Chl (Figure 2f). Given that the poly(HPMA)-Chl-PTA conjugate binds two small-molecule drugs, the release capacity of both small molecules was tested in solutions with and without DTT at pH 5 and 7.4, respectively. In the case of pH = 7.4 and without DTT, there was no significant release of Chl and 6MP (Figure 2g). When pH decreased to 5 and DTT increased to 20 μmol, the cumulative release of Chl and 6MP reached 80% and 75% after 25 hr, respectively. Subsequently, the pH and DTT concentration of the solution were adjusted to 1.0 and 1.0 mmol, respectively, and left for 30 min. The conjugate was freeze-dried to obtain the residue after 3 days of water dialysis. Interestingly, the characteristic absorption peaks of both Chl and 6MP disappeared in the residues (Figure 2h). The residue also lost its ability to self-assemble and turned into a random scattered structure (Figure 2i). This suggests that Chl and PTA in the conjugate can be released in the low pH and high GSH environment of cancer cells.

Blood safety is the primary requirement of a drug delivery system, and it is measured by hemolysis. Hemolysis rates falling within the ranges of 0–2%, 2–5%, and 5–100% were categorized as non-hemolytic, mildly hemolytic, and hemolytic, respectively.[32,33] In this work, the hemolysis tests of the poly(HPMA)-Chl-PTA conjugate were processed and summarized in Figure S5. PBS and pure water served as the positive and negative controls, which resulted in no hemolysis and significant hemolysis, respectively. Although the hemolysis rate increased with increasing concentration of the poly(HPMA)-Chl-PTA conjugate, it was less than 4.5% at all concentrations (Figure S5b). Furthermore, the conjugate shows mildly hemolytic even when the concentration increased to 500 μg/mL. The findings suggest that the conjugate did not cause any detrimental effects on red blood cells and demonstrated its excellent blood compatibility.

The CCK-8 method was used to detect the inhibitory effect of the three conjugates on HepG2 cell proliferation (Figure S6). The number of poly(HPMA)-PTA-Chl conjugate is fixed and the concentrations of poly(HPMA)-PTA and poly(HPMA)-Chl are subsequently adjusted, in order to make the concentrations of Chl in poly(HPMA)-PTA-Chl and poly(HPMA)-Chl are the same, and the concentrations of PTA in poly(HPMA)-PTA-Chl and poly(HPMA)-PTA are the same during cell experiments. The three conjugates exhibited concentration-dependent cytotoxicity to the cells at 24 hr. Based on these conditions, the cell survival rates were observed to decrease as the concentration gradually increased, and the IC_{50} values for poly(HPMA)-Chl, poly(HPMA)-PTA, and poly(HPMA)-PTA-Chl were 41.8, 43.5, and 25.58 μg/mL, respectively. To assess the combined effect of the drugs, the combination index (CI) was calculated to determine if both drugs exerted a synergistic effect within cells.[34,35] In this work, the CI value is about 0.81, which is notably lower than 1, indicating an obvious synergistic effect of Chl and 6MP on HepG2 cells.

The morphological alterations in HepG2 cells following their incubation with three different conjugates were characterized by fluorescence imaging (Figure 3). By subjecting the cell population to the three conjugates for 24 hr, various types of cells were observed, including early apoptotic cells (indicated by a blue color), late apoptotic cells (displaying a blue-violet color), and necrotic cells (appearing as red color).[36,37] The control group cells (Figure 3a) presented normal circular or elliptical shapes, smooth surfaces, clear edges, normal morphology, clear nuclear size and contour, and abundant cells visible in the field of view with good surface cell growth. The cells showed bright blue fluorescence, while the red fluorescence was almost imperceptible, indicating that the cells were alive. After 24 hr of incubation with the three conjugates, respectively, the number of cells showing red fluorescence increased significantly compared with the control group (Figure 3b–d). Both the pronounced blue fluorescence and the limited red fluorescence in Figure 3b and c suggest that the poly(HPMA)-PTA and poly(HPMA)-Chl conjugates are associated with the initial stages of apoptosis. As for the poly(HPMA)-Chl-PTA (Figure 3d), the strong blue and red fluorescence signals indicate an advanced stage of the apoptosis process, as evidenced by the ability of PI to permeate the cell membrane. The HepG2 cells, respectively, treated with the three conjugates exhibited a notably elevated intensity of blue fluorescence upon staining with Hoechst 33342 (Figure 3e), compared to the negative control $p < 0.0001$ (****). The fluorescence intensity observed in cells treated with poly(HPMA)-Chl-PTA was markedly greater than that, respectively, treated by poly-(HPMA)-PTA and poly(HPMA)-Chl conjugates. The significant red fluorescence intensity, observed in HepG2 cells treated with propidium iodide (Figure 3f), was exclusive to those treated with poly(HPMA)-Chl-PTA; $p < 0.01$ (**). In this way, a more standard expression for the synergistic effect offered by Chl and 6MP on HepG2 cells is obtained.

A more detailed observation of the induction of cell apoptosis by three different conjugates is carried out using the flow cytometry technology, and the related cell density maps are shown in Figure 4a–f. Compared to the control group (Figure 4a–c), significant signs of cell apoptosis were observed after treating with the three conjugates for 24 hr (Figure 4d–f).[38] The percentages of early-stage apoptotic HepG2 cells induced by poly(HPMA)-PTA, poly(HPMA)-Chl, and poly(HPMA)-Chl-PTA were 37.73%, 22.98%, and 52.92%, respectively, indicating the conjugation of poly(HPMA)-Chl-PTA results in a significantly higher early-stage apoptotic rate compared with the other two conjugations. Moreover, the percentages of late-stage apoptotic HepG2 cells induced by poly(HPMA)-PTA, poly(HPMA)-PTA, and poly(HPMA)-Chl-PTA were 1.29%, 2.90%, and 28.96%, respectively. This indicates that the co-delivery of the two drugs as conjugates greatly enhances the cytotoxicity against HepG2 cells.

In addition, the impact of the three conjugates on the cell cycle of HepG2 cells is also studied by PI staining. The cycle data of cells treated with three conjugates in G0/G1, S, and G2/M phases is summarized in Figure 4g–j. The G0/G1 value of the control group was approximately 69.69%. After treatment with the three conjugates, the values decreased to

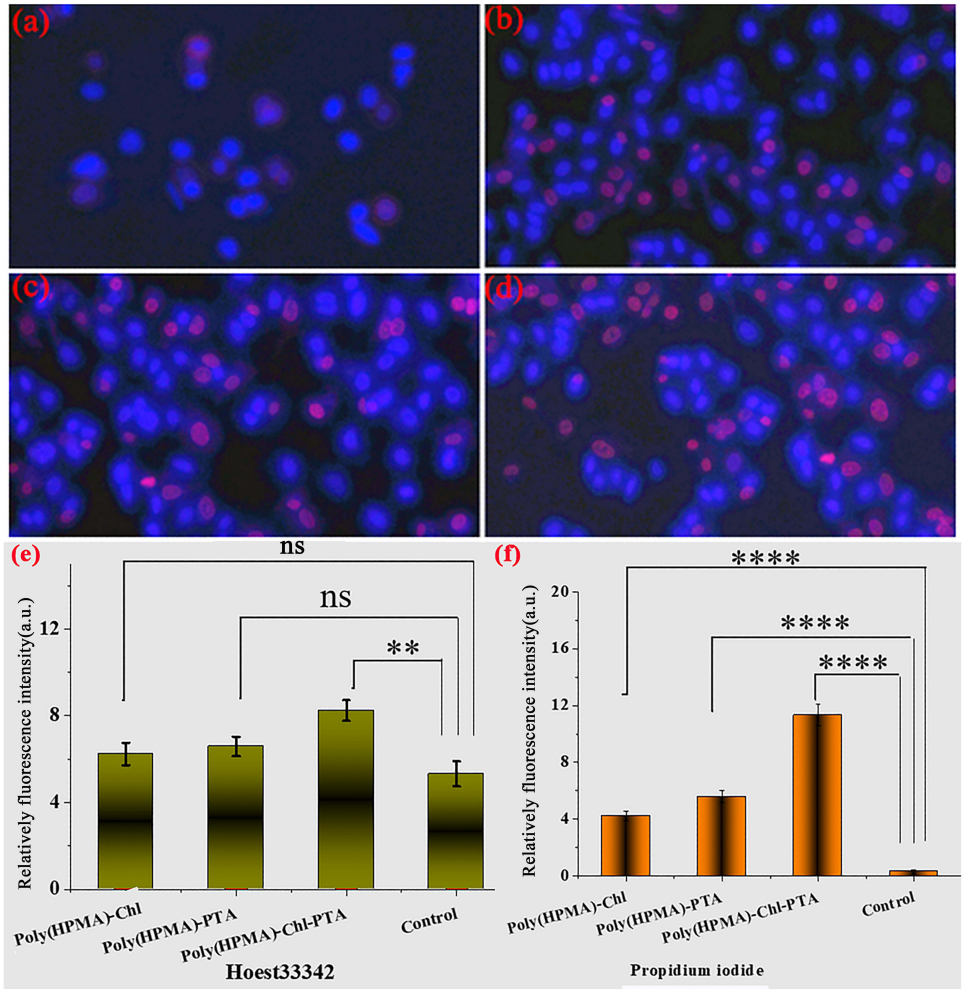

Figure 3 Merge confocal microscopy images of the cells incubated with different materials after 24 h of treatment: PBS (**a**), poly(HPMA)-Chl (**b**), poly(HPMA)-PTA (**c**) and poly(HPMA)-Chl-PTA (**d**). All the cells were stained by Hoechst 33324 and Propidium iodide, The images were merged after collecting the related images at the corresponding wavelength of Hoechst 33324 and Propidium iodide, respectively. Early and late apoptotic cells showed blue and red fluorescence, respectively. (**e** and **f**) are the relatively fluorescence intensity of the stained cells treated by Hoechst 33324 and Propidium iodide, respectively.

Notes: Significant differences (p) between the values were assessed using a one-way analysis of variance. ** means $p < 0.01$, **** means $p < 0.0001$ significant difference when comparing treated cells to control.

Abbreviation: ns, no significance.

60.30%, 64.55%, and 57.52%, respectively. Concurrently, the S phase value increased from 26.49% to 36.06%, 26.25%, and 38.44%, respectively. From these results, it can be concluded that the three conjugates can block HepG2 cells in the S phase. These results demonstrate the distinct advantage of the dual-loaded drug in preventing the S phase of the cell cycle and also indicate its better inhibitory impact on cell proliferation than that of the single-loaded ones.

The uptake of the conjugate into the cells was quantified after the cells were treated with cy5.5 labeled conjugate. As shown in Figure 4k–p, the update occurred in a time-dependent manner and finally achieved a plateau after 10 h at a final concentration of 25 μg Cy5.5/L. This could be attributed to the requirement of the conjugate to interact with specific receptors on the surface of the plasma membrane, leading to the formation of coated pits that facilitate its internalization into the cells. The conjugate progressively depleted the population of receptors present on the surface of the plasma membrane over time. In particular, the complex could be swallowed into cells and distributed in both cytoplasm and nuclei of HepG2 cells by emitting red fluorescence. The conjugates were mainly distributed in the nucleus and cytoplasm after entering the cell according to the fluorescent images, which was conducive to the release of the drug and its effect.

Subsequently, the metabolism and distribution of fluorescently labeled conjugate in vivo were studied on a small animal living imaging system. First, 50 μL volume of the conjugate (2 mg mL^{-1}) was administered via intravenous

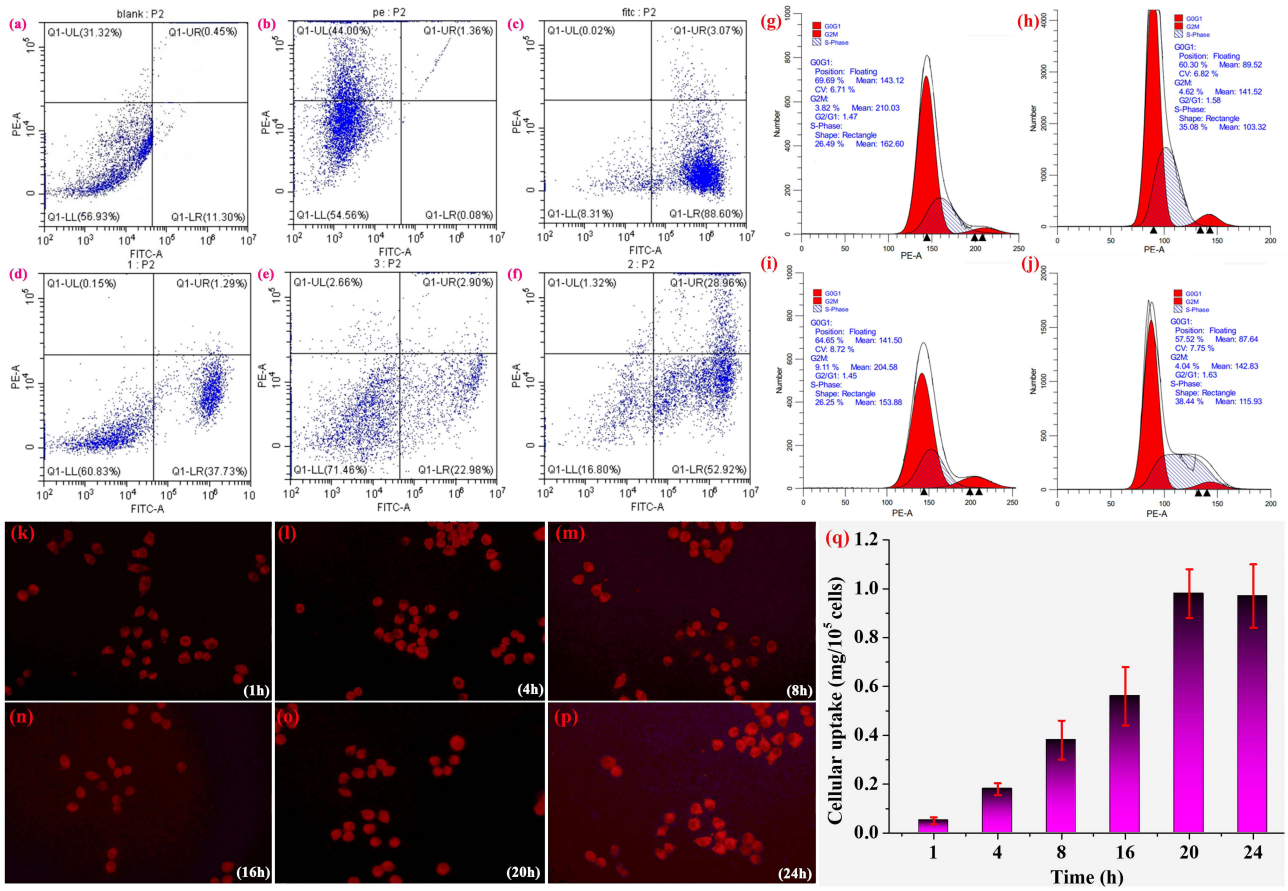

Figure 4 Flow cytometry analysis of cells after incubation with poly(HPMA)-PTA (**d**), poly(HPMA)-Chl (**e**) and poly(HPMA)-Chl-PTA (**f**), control group shown in (**a–c**); Cycle analysis of cells after incubation with control (**g**) and poly(HPMA)-PTA (**h**), poly(HPMA)-Chl (**i**), and poly(HPMA)-Chl-PTA (**j**); Fluorescence images of HepG2 cells incubated with Cy5.5 labeled poly(HPMA)-Chl-PTA conjugate at 1, 4, 8, 16, 20, 24 h; the fluorescence intensity (**q**) of the cellular uptake for different times.

injection into nude mice, followed by the monitoring of fluorescent signals at different time intervals (Figure 5a). At 0.5 hr after injection, a strong and discernible fluorescence signal was prominently observed throughout the entire body of the mice, exhibiting an impressive signal-to-noise ratio. This verified that the conjugate could efficiently penetrate the tissues of mice and circulate rapidly through the whole body. The fluorescence signal quickly spread throughout the whole body with the continuation of time, and the relative fluorescence intensity increased continuously and reached the peak at 8.0 hr after injection. The highest fluorescence intensity was on the order of magnitude of 10^8. Then, the fluorescence began to decline with time increase to 12 hr. The fluorescence signal became very weak after 12.0 hr. At 20 and 24 hr, a weak fluorescence signal was observed only at the kidney site of the mouse, while the fluorescence signal in other sites disappeared almost completely (Figure 5b). There were no observable acute toxicological reactions in any of the animals during the experiments.

The major organs of the mice, such as the liver, spleen, kidney, lung, stomach, and heart were extracted for ex vivo fluorescence imaging. Mean fluorescent intensity of these organs was quantitatively analyzed at 0.5 hr, 4.0 hr, 8.0 hr, and 24 hr post-injection (p.i.), respectively (Figure 5c). Strong fluorescent signals were observed from the liver and kidney at 4 and 8 h. After 24 hr p.i., the fluorescence signal of other major organs disappeared completely except the kidney. This phenomenon could be attributed to the small size of the conjugate, which enables it to permeate the glomerular cell membrane and be eliminated from the body through the urinary system. Figure 5d provides a more intuitive representation for the above discussion. It is clear that the conjugates mainly accumulate in the liver and kidney and gradually metabolize along with the increase in time. Finally, considering the high toxicity of Chl and 6MP, histological examination of organs with the H&E staining method was executed to evaluate the potential side effects (tissue damage, inflammation, and lesions) of

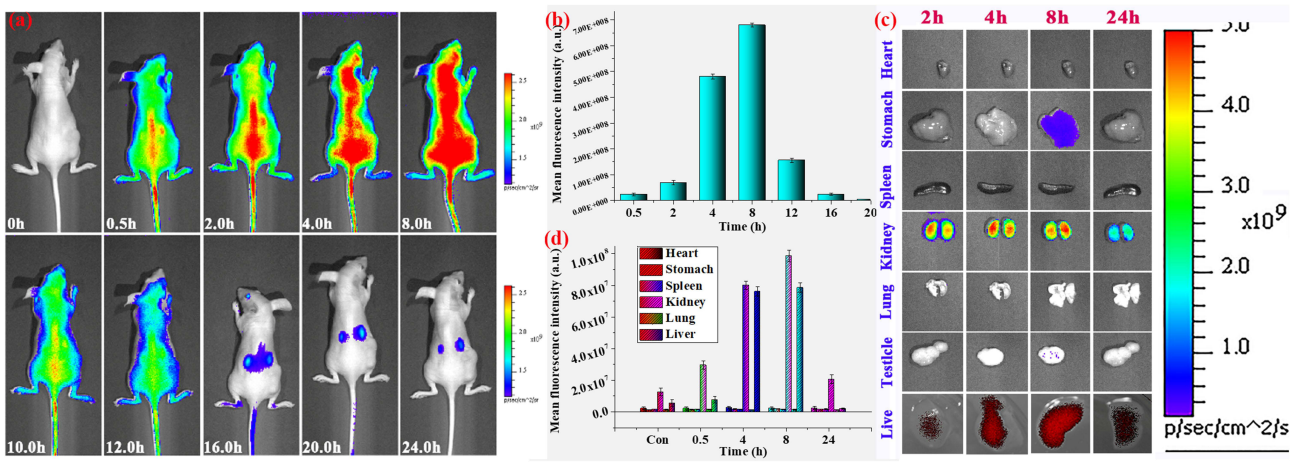

Figure 5 In (**a**) and ex vivo (**c**) imaging of mice with intravenous injection of the Cy5.5 labeled poly(HPMA)-Chl-PTA conjugate at different time points (n=3); the fluorescence intensity of the in (**b**) and ex vivo (**d**) for different time of Poly(HPMA)-Chl-PTA conjugate.

poly(HPMA)-Chl-PTA at a dosage of 10 mg kg^{-1}. Major organs (brain, heart, liver, lung, and kidney) were collected from mice after being injected for 7 days. No discernible histopathological abnormalities, degenerations, or lesions were detected (Figure S7), which may be due to the stability of the conjugate during the physiological environment. This implies that the conjugate exhibited no apparent toxicity in the mice as a prodrug system.

Conclusion

In conclusion, a polymer prodrug system was designed and prepared by introducing Chl and 6MP into the polyHPMA. Thus, the effective co-delivery of the two drugs was successfully realized. The prepared conjugate loaded 10.5% and 11.2% of chlorambucil and mercaptopurine, which can assemble into particles with a diameter of approximately 120 nm in aqueous solution. The conjugate nanoparticles can remain stable in aqueous media for at least 1 week. Overall, 65% of Chl and 78% of 6MP are released in pH of 5 and 20 μmol DTT at 12 h. The dual-drug loaded conjugate exhibited a combination index of 0.81 compared to the single-drug loaded conjugate, along with an increase in the ability to promote apoptosis in HepG2 cells and disrupt the cell division cycle by 2–5 times, demonstrating a significant synergistic effect. Fluorescence imaging of major organs conducted in vivo and ex vivo demonstrated that the dual-drug loaded conjugate was rapidly distributed throughout the entire body of mice, with a circulation time exceeding 24 hr. The main organs involved in its metabolism were found to be the liver and kidneys. After continuous administration for 5 days, the major organs of the mice showed no significant pathological damage. Moreover, the conjugate delivery system can be extended to integrate multiple different types of drugs into the same conjugate, achieving combination delivery of various drugs by controlling the drug loading amount and ratios. By leveraging the synergistic effects among different drugs, this approach could greatly enhance therapeutic efficiency.

Acknowledgments

The funding for this work is provided by the young talent innovation project of Lanzhou City (No: 2023-QN-59), the youth mentor fund (GAU-QDFC-2023-06) and scientific research start-up funds for doctors recruited openly (No. GAU-KYQD-2019-23) by Gansu Agricultural University.

Disclosure

The authors declare no competing interests in relation to this work.

References

1. Hu Q, Sun W, Wang C, Gu Z. Recent advances of cocktail chemotherapy by combination drug delivery systems. *Adv Drug Deliv Rev*. 2016;98:19–34. doi:10.1016/j.addr.2015.10.022
2. Ma L, Smith KM, Smith A. Andrew nanoparticles for combination drug therapy. *ACS Nano*. 2013;7(11):9518–9525. doi:10.1021/nn405674m

3. Zhang RX, Wong HL, Xue HY, et al. Nanomedicine of synergistic drug combinations for cancer therapy–strategies and perspectives. *J Control Release*. 2016;240:489–503. doi:10.1016/j.jconrel.2016.06.012
4. Pomeroy AE, Schmidt EV, Sorger PK, et al. Drug Independence and the curability of cancer by combination chemotherapy. *Trends Cancer*. 2022;8(11):915–929. doi:10.1016/j.trecan.2022.06.009
5. Woodcock J, Griffin JP, Behrman RE. Development of novel combination therapies. *N Engl J Med*. 2011;2011:364985–364987.
6. Liao L, Liu J, Dreaden EC, et al. A convergent synthetic platform for single-nanoparticle combination cancer therapy: ratiometric loading and controlled release of cisplatin, doxorubicin, and camptothecin. *J Am Chem Soc*. 2014;136(16):5896–5899. doi:10.1021/ja502011g
7. Detappe A, Nguyen HVT, Jiang Y, et al. Molecular bottlebrush prodrugs as next-generation mono and triplex combination therapies for multiple myeloma. *Nat Nanotechnol*. 2023;18(2):184–192. doi:10.1038/s41565-022-01310-1
8. Funasaki S, Mehanna D, Ma W, et al. Targeting chemoresistance in Xp11.2 translocation renal cell carcinoma using a novel polyamide–chlorambucil conjugate. *Cancer Sci*. 2022;113:2352–2367. doi:10.1111/cas.15364
9. Aputen AD, Elias MG, Gilbert J, et al. Potent chlorambucil-platinum(IV) prodrugs. *Int J Mol Sci*. 2022;23(18):28. doi:10.3390/ijms231810471
10. Akdogan Y, Sozer SC, Akyol C, et al. Synthesis of albumin nanoparticles in a water-miscible ionic liquid system, and their applications for chlorambucil delivery to cancer cells. *J Mol Liq*. 2022;367:11. doi:10.1016/j.molliq.2022.120575
11. Kumari S, Nehra A, Gupta K, et al. Chlorambucil-loaded graphene-oxide-based nano-vesicles for cancer therapy. *Pharmaceutics*. 2023;15(2):14. doi:10.3390/pharmaceutics15020649
12. Zou Y, Gao W, Jin H, et al. Cellular uptake and transport mechanism of 6-mercaptopurine nanomedicines for enhanced oral bioavailability. *Int J Nanomed*. 2023;18:79–94. doi:10.2147/IJN.S394819
13. de Beaumais TA, Medard Y, Amblard O, et al. Improved HPLC quantification of 6-mercaptopurine metabolites in red blood cells: monitoring data and literature analysis. *Int J Mol Sci*. 2022;23:12.
14. Wang L, Dai CL, Fang Y, et al. A drug/carrier dual redox-responsive system based on 6-mercaptopurine dimer-loaded cysteine polymer nanoparticles for enhanced lymphoma therapy. *Nano Res*. 2022;15(5):4544–4554. doi:10.1007/s12274-021-4037-0
15. Kalimuthu K, Lubin BC, Bazylevich A, et al. Gold nanoparticles stabilize peptide-drug-conjugates for sustained targeted drug delivery to cancer cells. *J Nanobiotechnol*. 2018;16:34. doi:10.1186/s12951-018-0362-1
16. Zou YR, Mei D, Yuan JJ, et al. Preparation, characterization, pharmacokinetic, and therapeutic potential of novel 6-mercaptopurine-loaded oral nanomedicines for acute lymphoblastic leukemia. *Int J Nanomed*. 2021;16:1127–1141. doi:10.2147/IJN.S290466
17. Ali BT, Mohammed HM. Preparation. characterization and preliminary cytotoxic evaluation of 6-mercaptopurine-coated biotinylated carbon dots nanoparticles as a drug delivery system. *Drug Des Dev Ther*. 2023;80:2327–2333.
18. Zhang M, Jin X, Gao M, et al. A self-reporting fluorescent salicylaldehyde–chlorambucil conjugate as a type-II ICD inducer for cancer vaccines. *Adv Mater*. 2022;34:36.
19. Salim SA, Kamoun EA, Evans S, et al. Mercaptopurine-loaded sandwiched tri-layered composed of electrospun polycaprolactone/poly(methyl methacrylate) nanofibrous scaffolds as anticancer carrier with antimicrobial and antibiotic features: sandwich configuration nanofibers, release study and in vitro bioevaluation tests. *Int J Nanomed*. 2021;16:6937–6955.
20. Monajati M, Tamaddon AM, Abolmaali SS, et al. L-asparaginase immobilization in supramolecular nanogels of PEG-grafted poly HPMA and bis (α-cyclodextrin) to enhance pharmacokinetics and lower enzyme. *Colloids Surf B Biointerfaces*. 2023;191:108802.
21. Yi X, Yue Shen YX, Li L, et al. Mitochondria-targeted delivery of camptothecin based on HPMA copolymer for metastasis suppression. *Pharmaceutics*. 2022;14:1534. doi:10.3390/pharmaceutics14081534
22. Monajati M, Tamaddon AM, Abolmaali SS, et al. Novel self-assembled nanogels of PEG-grafted poly HPMA wit-h bis(α-cyclodextrin) containing disulfide linkage: synthesis, bio-disintegration, and in vivo biocompatibility. *New J Chem*. 2022;46:9931–9943. doi:10.1039/D1NJ05974B
23. Li G, Zhao M, Zhang J, et al. Poly(HPMA)-chlorambucil conjugate nanoparticles: facile fabrication and in vitro anticancer activity. *New J Chem*. 2021;45:18544–18551. doi:10.1039/D1NJ03134A
24. Alfurhood JA, Sun H, Kabb CP, et al. Poly(N-(2-hydroxypropyl)methacrylamide)–valproic acid conjugates as block copolymer nanocarriers. *Poly Chem*. 2017;8(34):4983–4987. doi:10.1039/C7PY00196G
25. Saha B, Haldar U, De P. Polymer-chlorambucil drug conjugates: a dynamic platform of anticancer drug delivery. *Macromol Rapid Comm*. 2016;37:1015–1020. doi:10.1002/marc.201600146
26. Xu W, Li G, Long H, et al. Glutathione responsive poly(HPMA) conjugate nanoparticles for efficient 6-MP delivery. *New J Chem*. 2019;43(31):12215–12220. doi:10.1039/C9NJ02582K
27. Gunasekaran S, Kumaresan S, Arun Balaji R, et al. Vibrational spectra and normal coordinate analysis on structure of chlorambucil and thioguanine. *Pramana*. 2008;71(6):1291–1300. doi:10.1007/s12043-008-0183-0
28. Wei X, Liao J, Davoudi Z, et al. Folate receptor-targeted and GSH-responsive carboxymethyl-chitosan nanoparticles containing covalently entrapped 6-mercaptopuri-ne for enhanced intracellular drug delivery in leukemia. *Mar Drugs*. 2018;16:439. doi:10.3390/md16110439
29. Ebbesen MF, Schaffert DH, Crowley ML, et al. Synthesis of click-reactive HPMA copolymers using RAFT polymerization for drug delivery applications. *J Polym Sci Pol Chem*. 2013;51(23):5091–5099. doi:10.1002/pola.26941
30. Dhal PK, Polomoscanik SC, Gianolio DA, et al. Well-defined aminooxy terminated N-(2-hydroxypropyl) methacrylamide macromers for site specific bioconjugation of glycoproteins. *Bioconjugate Chem*. 2013;24(11):1967–1968. doi:10.1021/bc4002932
31. Callahan J, Kopeček J. Semitelechelic HPMA copolymers functionalized with triphenylphosphonium as drug carriers for membrane transduction and mitochondrial localization. *Biomacromolecules*. 2006;7(8):2347–2356. doi:10.1021/bm060336m
32. Rani S, Sahoo RK, Nakhate KT, et al. Biotinylated HPMA centered polymeric nanoparticles for bortezomib delivery. *Int J Pharm*. 2020;579:13. doi:10.1016/j.ijpharm.2020.119173
33. Wang F, Li N, Wang W, et al. A multifunctional, highly biocompatible, and double-triggering caramelized nanotheranostic system loaded with Fe_3O_4 and DOX for combined chemo-photothermal therapy and real-time magnetic resonance imaging monitoring of triple negative breast cancer. *Int J Nanomed*. 2023;18:881–897. doi:10.2147/IJN.S393507
34. Ghorbani M, Hamishehkar H. Redox and pH-responsive gold nanoparticles as a new platform for simultaneous triple anti-cancer drugs targeting. *Int J Pharm*. 2017;520(1–2):126–138. doi:10.1016/j.ijpharm.2017.02.008
35. Ianevski A, Giri AK, Aittokallio T. SynergyFinder 3.0: an interactive analysis and consensus interpretation of multi-drug synergies across multiple samples. *Nucleic Acids Res*. 2022;50:w739–w743. doi:10.1093/nar/gkac382

36. Xin J, Fu L, Wang J, et al. Influence of parameters on the death pathway of gastric cells induced by gold nanosphere mediated phototherapy. *Nanomaterials*. 2022;12:646. doi:10.3390/nano12040646
37. Rodríguez-Expósito RL, Reyes-Batlle M, Sifaoui I, et al. Isobenzofuran-1(3H)-one derivatives: amoebicidal activity and program cell death in Acanthamoeba castellanii Neff. *Biomed Pharmacother*. 2022;150:113062. doi:10.1016/j.biopha.2022.113062
38. Chen K, Cai H, Zhang H, et al. Stimuli-responsive polymer-doxorubicin conjugate: antitumor mechanism and potential as nano-prodrug. *Acta Biomater*. 2019;84:339–355. doi:10.1016/j.actbio.2018.11.050